Original Articles

Temporal trend of sclerophyllous forest deterioration in the Metropolitan Region of Chile: a spectral index-based approach

Marco A. Peña [ab*], **Catalina A. Solís** [a]

[a] Department of Geography, Universidad Alberto Hurtado, Santiago, Chile.

[b] Department of Geography, Friedrich Schiller University Jena, Jena, Germany.

Article Info

Received: 01.06.2026

Accepted: 03.09.2026

Published: 17-09-2026

Corresponding author: mapena@uahurtado.cl

How to cite: Peña M. A., Solís C. A. (2026). Temporal trend of sclerophyllous forest deterioration in the Metropolitan Region of Chile: a spectral index-based approach. BOSQUE, 47, e4715.

https://doi.org/10.4206/bosque.e4715

Abstract

The sclerophyllous forest of Chile's Metropolitan Region experienced intense anthropogenic and climatic pressure in recent decades. This study analyzed its deterioration trends between 1985 and 2024, identifying their spatiotemporal patterns through the complementary interpretation of spectral-index trend maps. We adapted normalized difference formulations of three spectral indices from multitemporal Landsat imagery acquired at five-year intervals. Thereafter, we standardized pixel-level temporal slopes by forest subtype to classify change magnitude relative to vegetation cover and topography. The modified NDDI (normalized difference drought index) was sensitive to vegetation water stress, reaching its highest values in 2020 during the peak of the central Chile megadrought and declining in 2024 following increased precipitation. The strongest deterioration occurred in the southwestern study area, mainly affecting denser, more accessible stands at lower elevations and gentler slopes.

Keywords: forest degradation, Landsat imagery, megadrought, drought index, Mediterranean ecosystem.

Introduction

The sclerophyllous forest of central Chile comprises mesic and xeric evergreen species adapted to the hot, dry summers of the Mediterranean climate. Their tough leaves and deep root systems confer resistance to drought and wildfire (Peñuelas et al., 2017; Luebert and Pliscoff, 2018). Because this type of climate favors human settlement, these forests have long experienced anthropogenic pressures linked to land-use change and fragmentation, compounded by increasing aridity, warming, and associated drought stress (Schulz et al., 2011; Peñuelas et al., 2017; Miranda et al., 2020, 2023; González-Reyes et al., 2024). Together, these stressors have reduced forest resilience and promoted deforestation and degradation (Gao et al., 2020; Smith-Ramírez et al., 2023).

In central Chile, sclerophyllous forest is the dominant native forest and provides essential ecosystem services in a drought- and wildfire-prone region, including erosion control, groundwater recharge, biodiversity conservation, pollination, climate regulation, and carbon storage (Peñuelas et al., 2017; Smith-Ramírez et al., 2023). Approximately 60% of its potential distribution has been lost (Luebert and Pliscoff, 2018; Miranda et al., 2017). In some periods, deforestation rates ranked among the highest for native forests in central and southern Chile, making it one of the most transformed non-Amazonian ecosystems in South America (Salazar et al., 2015). Most remaining stands are degraded secondary forests, often dominated by savanna-like thorn scrub, whereas better-preserved stands persist mainly in mountainous and riparian environments (Miranda et al., 2015, 2017; Garfias et al., 2018).

Satellite remote sensing is key for monitoring forest degradation through synoptic large-area observations (West et al., 2019; Gao et al., 2020). Landsat is particularly valuable because of its long, consistent archive, widely used to monitor long-term forest productivity, biomass, and vigor (Joseph et al., 2011; Gao et al., 2020). Spectral indices employed in this context include the normalized difference vegetation index (NDVI) and normalized difference water index (NDWI), representing vegetation vigor and water content, respectively (West et al., 2019). More recently, the normalized difference drought index (NDDI) combines these indices to integrate structural and hydrological information, showing greater sensitivity to water stress than either index alone (Gu et al., 2007). Studies in Mediterranean, arid, and semi-arid ecosystems showed that high NDDI values precede severe drought and wildfire events and improve ecological modeling of drought-induced degradation (Stamou et al., 2025; Mahmoud et al., 2025).

In central Chile, NDVI time series have revealed widespread recent deterioration of sclerophyllous forests. Miranda et al. (2023) showed that, among the five Mediterranean-climate regions worldwide, central Chile exhibited the most extensive and synchronous productivity declines between 2000 and 2021. Approximately 39% of the forest declined significantly, culminating in a 2019 browning event affecting >90% of the forest across 2,360 km^2 in <100 days. Garreaud et al. (2025) likewise identified 2019 as an extreme drought year in which vegetation response became nonlinear under severe precipitation deficits. Topography and soil water availability are key factors modulating these responses, with forests in moist ravines more resilient than those on drier slopes and piedmonts (Miranda et al., 2020, 2023; Fuentes et al., 2025).

Central Chile was affected by a megadrought from 2010 to 2022, with temperature and precipitation anomalies exceeding those of comparable Mediterranean ecosystems (Miranda et al., 2023). In particular, 2019 and 2021 were hyperdrought years, with precipitation deficits exceeding 75% and causing major socio-environmental impacts (Garreaud et al., 2025). Since 2023, rainfall partially recovered following the end of the “La Niña” event (Garreaud, 2023; Dirección Meteorológica de Chile [DMC], 2026), potentially relieving vegetation water stress (Fuentes et al., 2025). The Metropolitan Region in central Chile is a clear case of sclerophyllous forest deforestation and degradation, largely driven by the expansion of Santiago, a city that concentrates ∼42% of the country’s population (Instituto Nacional de Estadísticas [INE], 2024). The Region currently contains only 2.5% of the national extent of this forest, underscoring the importance of conserving its remaining fragments and ecosystem services (Corporación Nacional Forestal [CONAF], 2024).

This study analyzes deterioration trends in the sclerophyllous forest of Chile’s Metropolitan Region over the last four decades (1985-2024) by identifying their spatiotemporal patterns through the complementary interpretation of spectral-index trend maps. To this end, we propose adapted NDVI and NDWI formulations to derive a vegetation drought index based on NDDI while avoiding numerical instabilities affecting their temporal-trend interpretation. We hypothesize that the sclerophyllous forest of the Metropolitan Region has undergone significant deterioration, with magnitudes varying among forest subtypes according to vegetation cover and topography. Specifically, the objectives are to: (1) characterize temporal variability in vegetation vigor, water status, and dryness in the main forest subtypes; (2) estimate temporal trends in these indices; and (3) analyze their spatiotemporal patterns relative to vegetation cover and topography.

Methods

Study area. The sclerophyllous forest targeted in this study is located in Chile's Metropolitan Region (Figure 1), largely bounded by the Maipo River basin. Its east-west extent (70°45′-71°45′ W) ranges from the Andean piedmont to the Coastal Range spurs, and north-south (33°05′-34°00′ S) from the Chacabuco Range to the Angostura de Paine spur of the Coastal Range.

The Region has a Mediterranean climate, with a mean annual temperature of ∼14 °C and January averages of ∼22 °C, the warmest month. Mean annual precipitation is ∼369.5 mm, decreasing from the coast toward the Central Valley and increasing toward the Andes because of orographic uplift. During the 2010-2022 megadrought, precipitation declined by ∼80%, intensifying water stress and reducing forest productivity (Miranda et al., 2020; Smith-Ramírez et al., 2023; Fuentes et al., 2025).

Dominant tree species include peumo (*Cryptocarya alba* Molina), quillay (*Quillaja saponaria* Molina), litre (*Lithraea caustica* (Molina) Hook. & Arn.), boldo (*Peumus boldus* Molina), and espino (*Acacia caven* (Mol.) Mol.). Species of conservation concern include the Vulnerable northern belloto (*Beilschmiedia miersii* Gay), algarrobo (*Neltuma chilensis* (Molina) C.E. Hughes & G.P. Lewis), and northern oak (*Nothofagus macrocarpa* (A. DC.) F.M. Vázquez & R.A. Rodríguez), and frangel (*Kageneckia angustifolia* D. Don), listed as Near Threatened (Ministerio del Medio Ambiente [MMA], 2025).

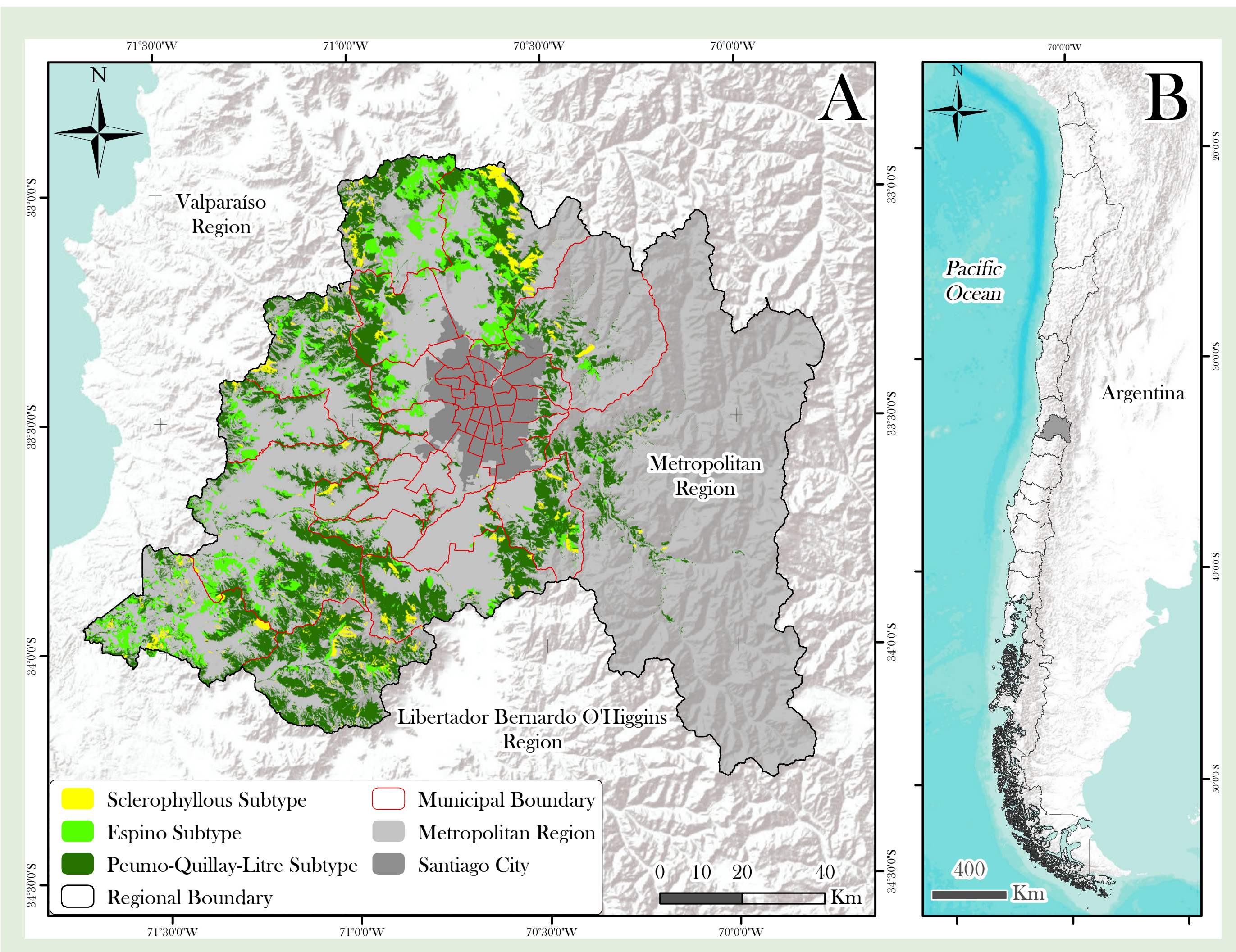

Figure 1. Study area (A), including the three dominant sclerophyllous forest subtypes of Chile's Metropolitan Region, and its Regional location within Chile (B). Source: CONAF (2024).

Materials. Because this study focused on forest deterioration rather than complete vegetation loss (deforestation), sclerophyllous forest subtypes were delineated from their current distribution and analyzed retrospectively from 1985 to 2024. For this purpose, the 2019 update of the Land Use and Vegetation Cadaster was used (CONAF, 2024), which recognizes seven sclerophyllous forest subtypes: Peumo-Quillay-Litre (PQL), Espino, Sclerophyllous, Frangel, Algarrobo, Riparian, and Belloto. We focused on the first three as they represent 99% of the regional extent (Table 1).

To minimize edge effects associated with spectrally mixed pixels at the boundaries of the forest subtype polygons, an inner buffer corresponding to the Landsat spatial resolution was applied (Table 2).

We also used the vegetation cover layer of the cadaster, classifying forest cover into five categories: dense, semi-dense, open, very open, and sparse.

To maximize temporal coverage, we assembled a Landsat image set using Collection 2 Tier 1 Level 2 products, providing atmospherically corrected surface reflectance at 30 m spatial resolution. We selected nine images from EarthExplorer (U.S. Geological Survey, 2026) following a five-year interval sampling beginning in 1985 (earliest year available for the study area), seeking to balance long-term coverage and temporal representativeness. All images were acquired in January, the only summer month with complete cloud-free coverage for all the years (Table 3).

Table 1. Main characteristics of the three dominant sclerophyllous forest subtypes in the Metropolitan Region of Chile.

Forest subtype	Description
Peumo-Quillay-Litre (PQL)	Multi-structural forest formations of variable density, composed in their upper canopy mainly of *Cryptocarya alba* Molina, *Quillaja saponaria* Molina, and *Lithraea caustica* (Molina) Hook. & Arn., in association with other species such as *Peumus boldus* Molina and *Kageneckia oblonga* Ruiz & Pav. The latter are also present as shrubs in the understory, together with numerous herbaceous plants adapted to low-moisture conditions.
Espino	Savanna-like formations that are predominantly mono-structural, characterized by trees and shrubs of espino (*Acacia caven* (Mol.) Mol.). Secondary species include a variety of drought-resistant herbs and shrubs such as *Retanilla trinervia* (Gillies & Hook.) Hook. & Arn. and *Schinus latifolius* (Gillies *ex* Lindl.) Engl., associated with *Maytenus boaria* Molina.
Sclerophyllous	Forest formations composed of evergreen hard-leaved trees and shrubs, capable of forming a continuous upper canopy with a diverse understory of drought-adapted shrubs and herbs. The commonly dominant species are *Peumus boldus* Molina and *Kageneckia oblonga* Ruiz & Pav., followed by *Quillaja saponaria* Molina and *Lithraea caustica* (Molina) Hook. & Arn.

Source: Gajardo (1994); Luebert and Pliscoff (2018).

Table 2. Area and number of patches of the three dominant sclerophyllous forest subtypes before and after 30 m inner buffering.

Forest Subtype	Area (km^2)		# patches	
	Original boundary	Buffered boundary	Original boundary	Buffered boundary
Peumo-Quillay-Litre (PQL)	2,628.86	2,062.97	20,346	17,364
Espino	804.25	617.36	2,827	2,361
Sclerophyllous	273.90	188.59	2,012	1,493

To characterize the climatic context throughout the study period, annual precipitation and annual mean maximum temperature were compiled from the meteorological stations with continuous records in the Metropolitan Region: Pudahuel, Tobalaba/Cerrillos, and Quinta Normal (Figure 2; DMC, 2026).

Finally, we downloaded a 12.5 m ALOS (Advanced Land Observing Satellite) digital elevation model (Centro de Información de Recursos Naturales [CIREN], 2016) to extract terrain elevation and derive slope and aspect.

Table 3. Acquisition dates of the Landsat images used.

Mission / Sensor	Acquisition date
Landsat-5 / Thematic Mapper (TM)	January 25, 1985
	January 10, 1991
	January 26, 1997
	January 5, 2001
	January 16, 2005
	January 30, 2010
Landsat-8 / Operational Land Imager (OLI)	January 12, 2015
	January 10, 2020
	January 21, 2024

Methods. We tracked the condition of the three forest subtypes using spectral indices derived from NDVI, NDWI, and NDDI formulations, the latter not previously used in Chilean vegetation ecology. They are based on normalized differences between spectral bands or indices themselves. NDVI and NDWI normalize the near-infrared band, sensitive to foliage abundance, using the red band and a shortwave infrared band, sensitive to foliar chlorophyll and water content, respectively. Similarly, NDDI normalizes NDWI using NDVI.

In their original formulation, these indices range between -1 and 1. While for NDVI and NDWI higher values indicate greater abundance of the variable they target, for NDDI they indicate increasing vegetation dryness. We reformulated them as normalized ratios by removing numerator subtraction, constraining them to [0, 1]. This modification reduced numerical amplification caused by small denominators in the original NDDI, avoiding extreme values that could hinder temporal-trend interpretation. Extending this reformulation to NDVI and NDWI also prevented near-zero denominators in the modified NDDI caused by opposite signs in the input indices. These modified indices are referred to as NVI, NWI, and NDI (Table 4).

For each forest subtype, spectral-index pixel values at each date were standardized relative to the multitemporal series [1]:

$$IEz_i = (IE_i - \mu IE)/\sigma IE \quad [1]$$

where IE_i is the index value at a given date, and μIE and σIE are the mean and standard deviation of the multitemporal index series.

Temporal slopes were then estimated at the pixel level using simple linear regression against time [2].

Table 4. Original and modified spectral-index formulations used in this study.

Category	Name	Notation	Formulation	Reference	Modified formulation
Vigor state	Normalized difference vegetation index	NDVI	(NIR-red) / (NIR+red)	Rouse et al. (1973)	NIR / (NIR+red)
Hydric state	Normalized difference water index	NDWI	(NIR-SWIR) / (NIR+SWIR)	Hunt et al. (1987)	NIR / (NIR+SWIR*)
Drought state	Normalized difference drought index	NDDI	(NDVI-NDWI) / (NDVI+NDWI)	Gu et al. (2007)	NVI / (NVI+NWI)

*First Landsat SWIR band.

$$IE\beta = (n \times \Sigma(x_i \times IE_{zi}) - \Sigma x_i \times \Sigma IE_{zi})/(n \times \Sigma x_i^2 - (\Sigma x_i)^2) \quad [2]$$

where n is the number of images in the series, x_i is time in days since the first acquisition date (January 25, 1985), and IEz_i are the standardized index values obtained from the preceding formula.

The resulting slope values ($IE\beta$) were subsequently standardized using the spatial mean and standard deviation of each forest subtype to express relative change. Standardized temporal-change values were defined independently for each forest subtype and grouped into six magnitude classes (Table 5): strong decrease, moderate decrease, slight decrease, slight increase, moderate increase, and strong increase. As such, these classes do not imply statistical significance of individual pixel-level regression slopes.

Classes were mapped using median vegetation cover and mean terrain elevation (m a.s.l.), slope (°), and aspect (°).

To assess differences among temporal-change classes, we performed one-way analyses of variance (ANOVA) for continuous variables (elevation, slope, and aspect) and chi-square tests for vegetation cover. Residual normality and variance homogeneity were adequate for ANOVA and subsequent comparisons. Analyses were conducted independently for each forest subtype and spectral

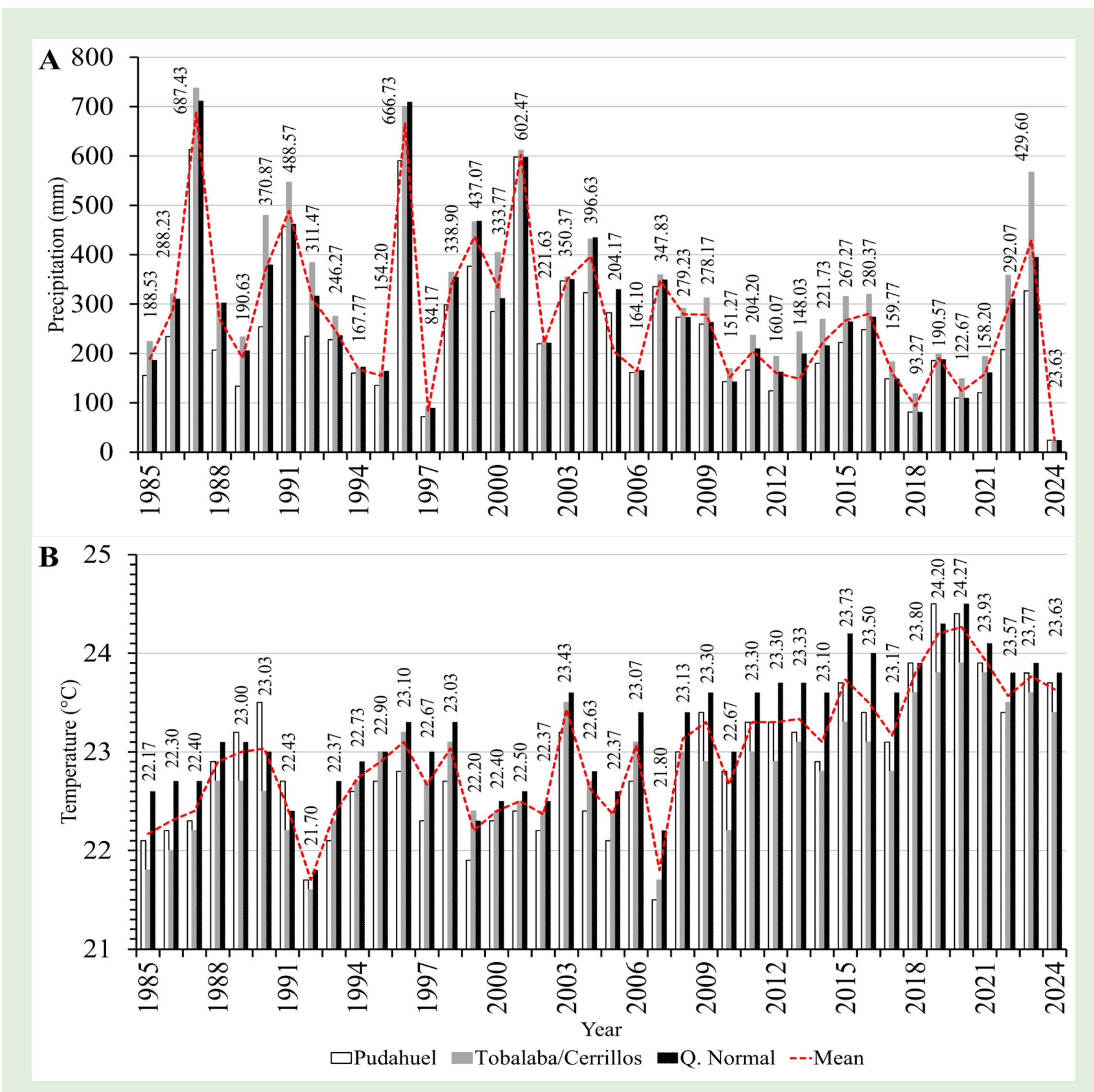

Figure 2. Annual precipitation (A) and maximum temperature (B) at the three meteorological stations of the Metropolitan Region (Pudahuel, Tobalaba, and Quinta Normal) and means for the selected years. Source: DMC (2026).

index. Variables were summarized at the patch level using means and modes for continuous and categorical variables, respectively. When significant ($P < 0.05$), Tukey's honestly significant difference (HSD) test identified significantly different category pairs.

Results

Reformulation of the original spectral indices. Table 6 shows the numerical effects of reformulating the normalized difference indices. Descriptive statistics for the three forest subtypes combined show that the modification constrained them to [0, 1]. NVI and NWI preserved a near-perfect and perfect correspondence with their original versions (mean correlations across the nine image dates of 0.97 and 1.00, respectively), retaining their spatial and temporal structure. In contrast, the original NDDI exhibited extreme values due to denominator instability, substantially attenuated after reformulation, yielding an NDI that no longer showed a linear correspondence with the original version (mean correlation across the nine image dates= 0).

Table 5. Intervals used to classify standardized temporal slopes of each spectral index.

Interval*	Temporal change magnitude class
< -1	Strong decrease
-1 < x ≤ -0.5	Moderate decrease
-0.5 < x ≤ 0	Slight decrease
0 < x ≤ 0.5	Slight increase
0.5 < x ≤ 1	Moderate increase
> 1	Strong increase

* For the NDI, the intervals are interpreted in reverse.

Table 6. Descriptive statistics of the normalized difference indices (NDVI, NDWI, and NDDI) and their modified formulations (NVI, NWI, and NDI) for the three forest subtypes combined during the study period, and correlations between corresponding pairs. $\bar{x}$= mean; σ= standard deviation; r= correlation.

Spectral index	Mean value of all image dates					
	Descriptive statistic				*r*	
	$\bar{x}$	σ	Min.	Max.	$\bar{x}$	σ
NDVI	0.39	0.14	-0.46	0.88	0.968	0.049
NVI	0.70	0.07	0.29	0.94		
NDWI	0.00	0.13	-0.49	0.76	1.000	0.000
NWI	0.50	0.06	0.25	0.88		
NDDI	2.71	2,387.30	-820.09	4,998.17	0.002	0.003
NDI	0.58	0.02	0.32	0.72		

Temporal behavior of standardized spectral indices. Standardized NVI and NWI means fluctuated over time, remaining mostly within ±1 standard deviation (Figure 3). In contrast, standardized NDI remained predominantly negative until 2015 and became positive at the two subsequent dates.

Negative standardized NDI values were associated with favorable water conditions, whereas positive values indicated drier conditions. For the forest as a whole, the highest value occurred in 2020 (1.83), coinciding with a marked NWI decline (-1.50) relative to NVI (-0.10).

The climatic context of the image acquisition dates is represented in Figure 2. Because the images were acquired in January, the vegetation conditions captured in each image are expected to reflect the cumulative influence of annual precipitation and annual mean maximum temperature during the preceding seasons. The time series shows that the most severe phase of the 2010-2022 megadrought occurred between 2015 and 2020, coinciding with the highest NDI values and with widespread water stress affecting this forest type (Miranda et al., 2023; Fuentes et al., 2025; Garreaud et al., 2025).

Spectral-index temporal trends. Grouping standardized temporal slopes of each index into six magnitude classes showed approximately symmetrical area distributions among forest types, with the intermediate classes accounting for ~40% of the total area (Figure 4).

NVI decreases were more frequent in the southwestern study area, whereas increases were more frequent along Coastal Range and Andean piedmont spurs in the northern study area (Figure 5).

NWI showed similar patterns, although decreases extended farther north, while increases were largely restricted to the Andean piedmont and central spurs of the Coastal Range (Figure 6).

Like NVI, NDI increases were most frequent in the northern study area. Decreases, however, were concentrated in the Andean piedmont and central spurs of the Coastal Range rather than in the southwestern study area (Figure 7).

Characterization of spatiotemporal deterioration patterns. Decreasing spectral-index temporal trends for the PQL subtype tended to occur in

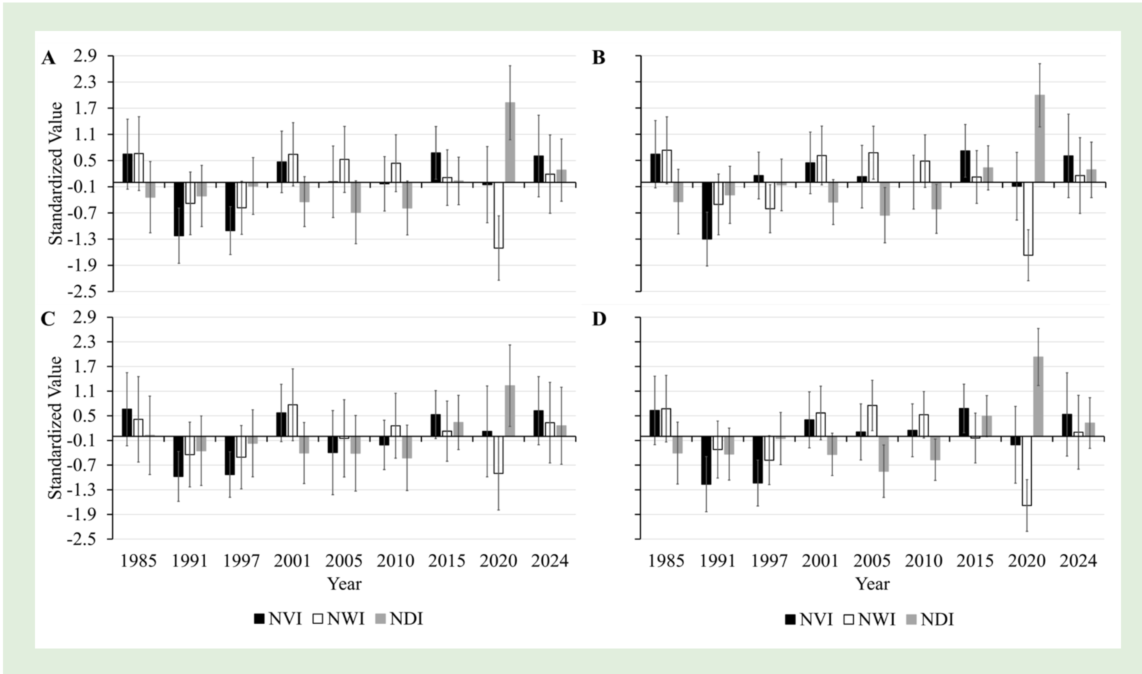

Figure 3. Temporal behavior of standardized spectral indices for the three forest subtypes combined (A) and separately: Peumo-Quillay-Litre (PQL) (B), Espino (C), and Sclerophyllous (D).

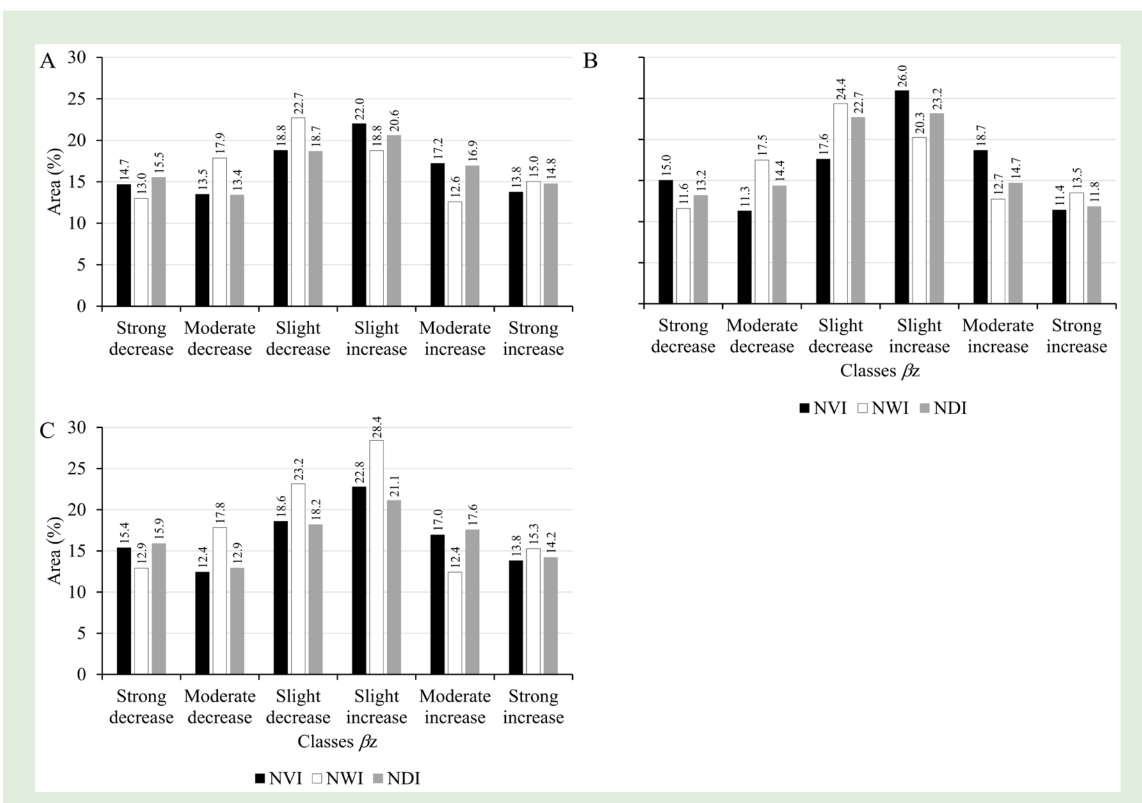

Figure 4. Area distribution (%) of six standardized spectral-index temporal-change classes for Peumo-Quillay-Litre (PQL) (A), Espino (B), and Sclerophyllous (C).

denser vegetation cover (class 2: Semi-dense) than in other subtypes (Figure 8A). In Espino, the Open cover class predominated across all temporal-change classes (Figure 8B), whereas in the Sclerophyllous subtype, Semi-dense (class 2) and Open (class 3) cover alternated across change classes (Figure 8C).

Figure 9 shows that the highest vegetation cover classes were concentrated in the southwestern study area, coinciding with strongest decreases in spectral-index temporal trends.

Elevation generally decreased with increasingly negative spectral-index temporal trends across the three forest subtypes (Figure 10). The figure also highlights distinct elevational ranges among subtypes, highest in Sclerophyllous (600-1,281 m a.s.l.; Figure 10C) and lowest in Espino (277-783 m a.s.l.; Figure 10B).

Espino showed the clearest relationship between spectral-index trends and slope, which decreased with increasingly negative trends (15.1-8.2° for NVI, 18.3-7.9° for NWI, and 16.4°-10.9° for NDI; Figure 11). Likewise, the strongest NVI and NWI decreases tended to occur on southwestern aspects, whereas NDI showed the opposite pattern (Figure 12).

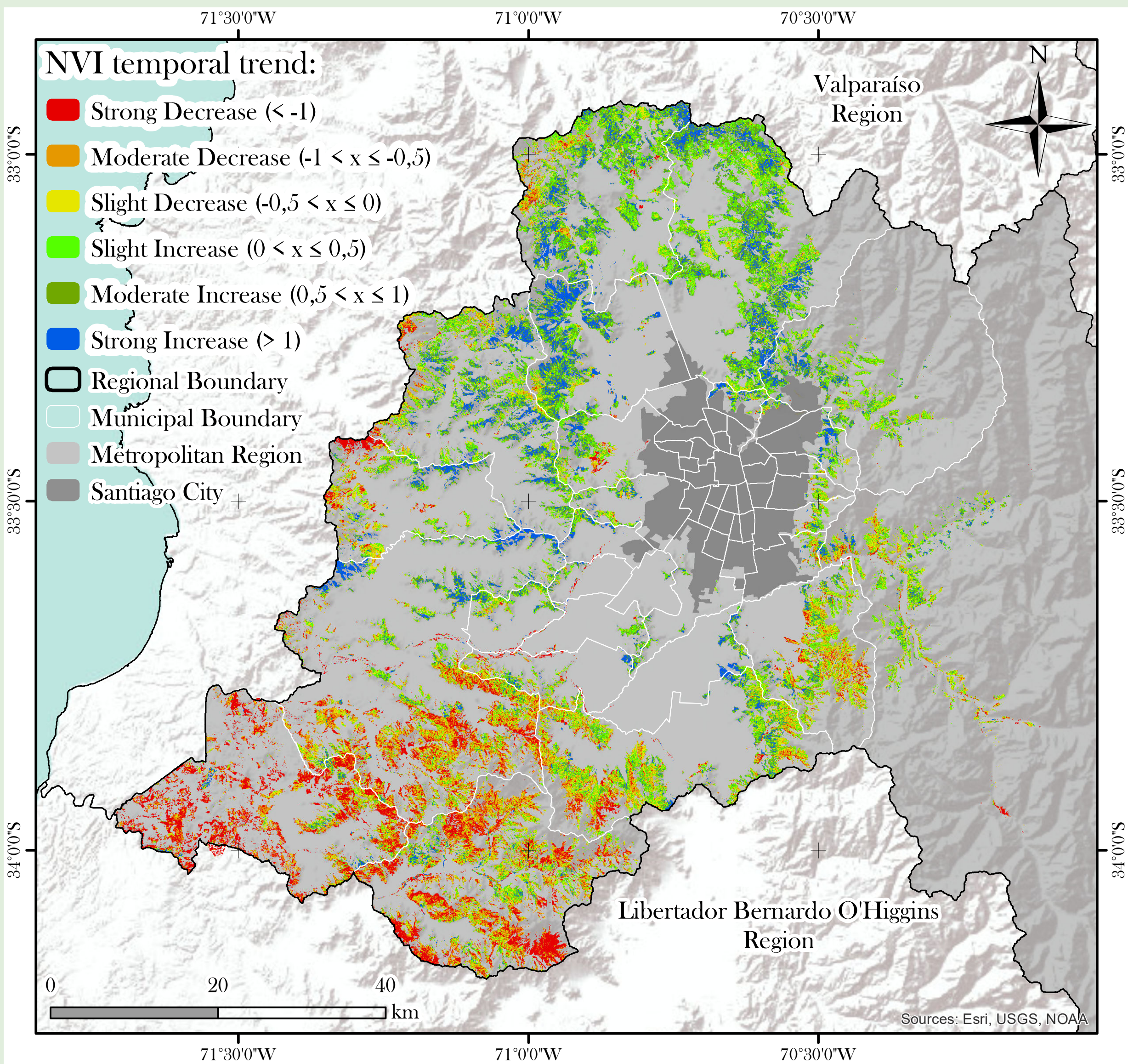

Figure 5. Spatial distribution of standardized NVI trends for the three forest subtypes.

Statistical relationships between spectral-index temporal trends and characterizing variables. ANOVA revealed significant differences between temporal-change classes and topographic variables, with varying strength among forest subtypes (Table 7). In general, increasing trends were associated with higher elevations and steeper slopes, whereas decreasing trends predominated at lower elevations and gentler slopes, particularly in the Sclerophyllous and PQL subtypes. These relationships were strongest for PQL (F = 171.3 for NVI, 123.1 for NWI, and 287.6 for slope).

Tukey's post hoc tests revealed that classes with strongest decreases in temporal trends exhibited greater predominance of southwestern aspects, whereas increasing classes occupied more varied exposures. This pattern was strongest for NDI, especially in Espino and PQL.

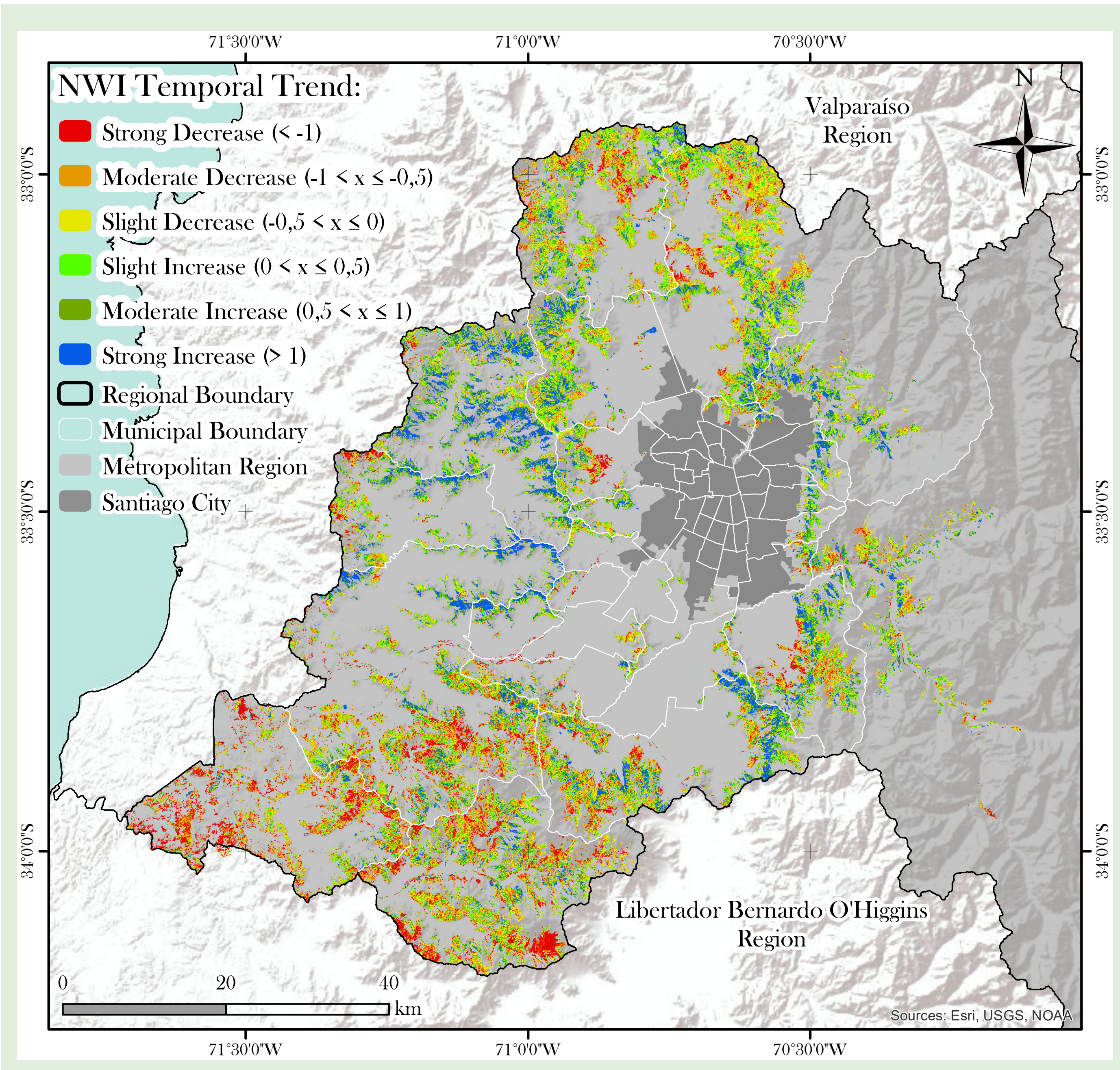

Figure 6. Spatial distribution of standardized NWI trends for the three forest subtypes.

Chi-square tests also revealed significant associations between temporal-change classes and vegetation cover. Stronger NVI and NWI decreases were associated with denser vegetation cover in Sclerophyllous and PQL, whereas more open cover predominated in Espino. NDI associations were significant only in Espino and PQL.

Discussion

This study extended the use of the NDDI to central Chile's Mediterranean environment to detect sclerophyllous forest deterioration. Under the eco-climatic conditions of the study area, however, the similar magnitudes of the NDVI and NDWI frequently

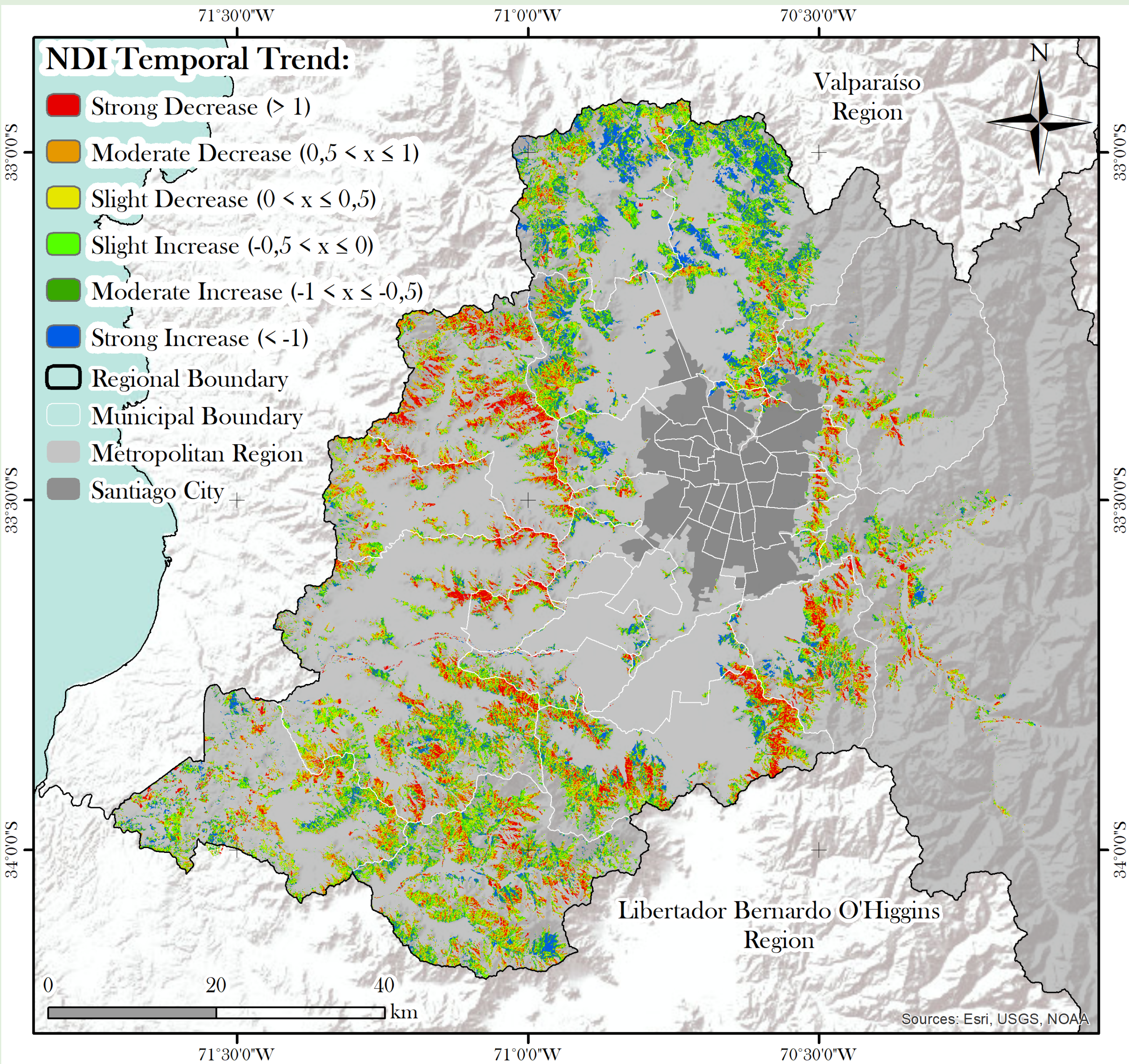

Figure 7. Spatial distribution of standardized NDI trends for the three forest subtypes.

yielded unstable NDDI values that limited its suitability for temporal analyses. To overcome this limitation, we reformulated the indices by expressing them on a continuous positive scale. Although this modification altered the numerical values of the original NDDI, it preserved the relative relationship between its component indices, as supported by the strong monotonic correspondence between the original and reformulated NDVI and NDWI. Consequently, the conceptual basis of the index remained unchanged, continuing to integrate complementary information on vegetation vigor and water content.

Standardized mean NDI values remained negative until 2015, consistent with the progressive decline in NWI. This pattern shifted abruptly in 2020, when NDI became positive during the 2019 hyperdrought (Garreaud et al., 2025), reflecting an imbalance between vegetation vigor and water availability. As water stress increased, NWI declined more sharply than NVI, increasing NDI and suggesting intensified vegetation dryness. Positive NDI values therefore indicated drier conditions relative to the study-period mean. Values observed in 2020 were consistent with the marked decline in NWI relative to NVI and cumulative megadrought effects since 2010. It coincided with massive synchronous foliar browning reported by Miranda et al. (2023) and the sharp reduction in primary productivity documented by Fuentes et al. (2025). This pattern partially reversed by 2024, when both indices increased

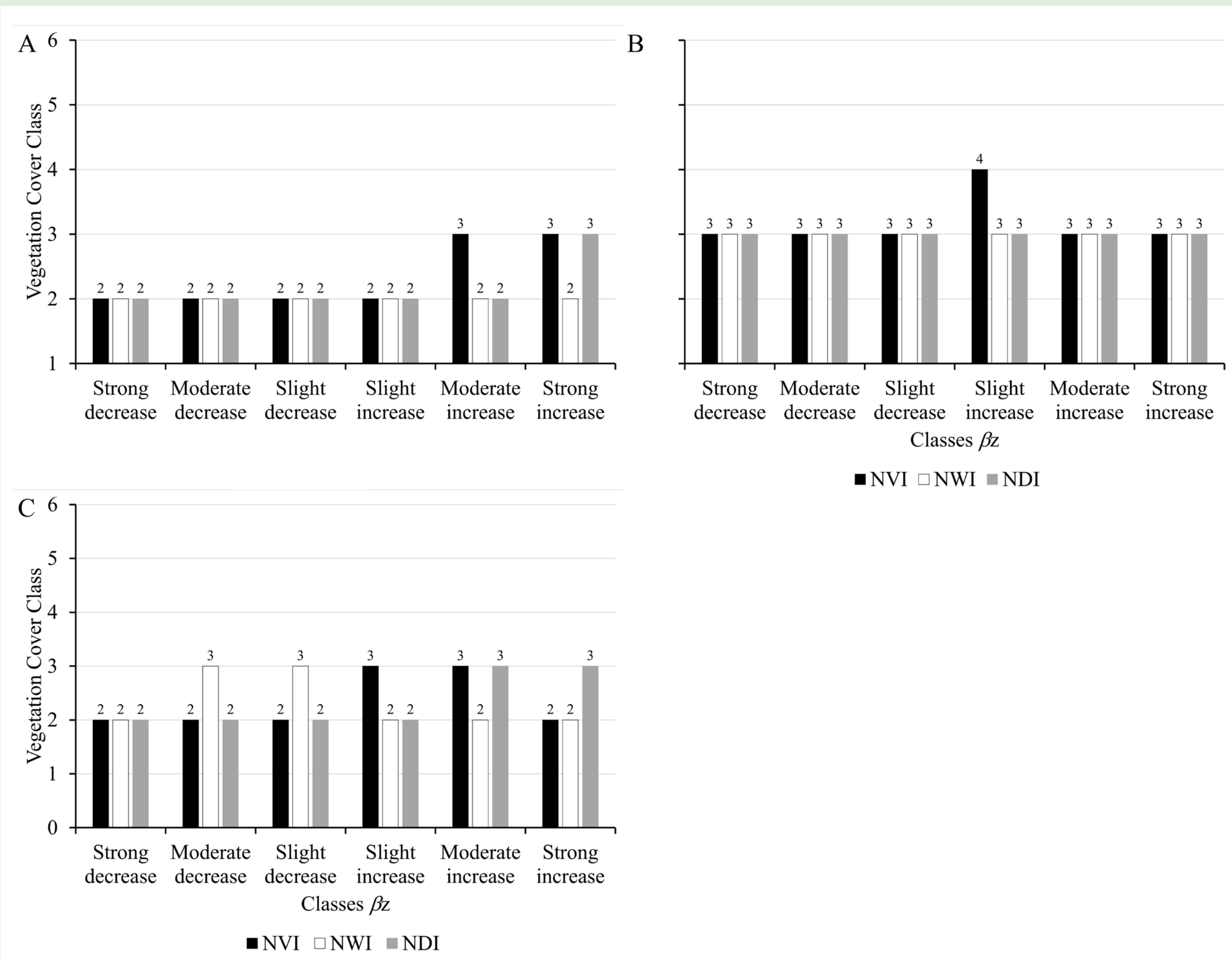

Figure 8. Dominant vegetation cover class by temporal-change class of standardized spectral-index trends for Peumo-Quillay-Litre (PQL) (A), Espino (B), and Sclerophyllous (C). Vegetation cover classes: (1) Dense, (2) Semi-dense, (3) Open, (4) Very Open, and (5) Sparse.

substantially, consistent with precipitation recovery in central Chile beginning in 2023 (Garreaud, 2023). Mean annual precipitation in the Metropolitan Region during 2023-2024 increased by 163.4% relative to 2018-2022 and 93.1% relative to the full megadrought period (2010-2022), during which no year exceeded 200 mm (DMC, 2026). This recovery likely reduced water stress and coincided with the first signs of partial ecosystem recovery reported by Fuentes et al. (2025).

Together with Garreaud et al. (2025), our findings reinforce that vegetation response becomes nonlinear under hyperdrought conditions. Consequently, NDI may help evaluate climate-driven water stress in Chilean sclerophyllous forests, whose recent deterioration

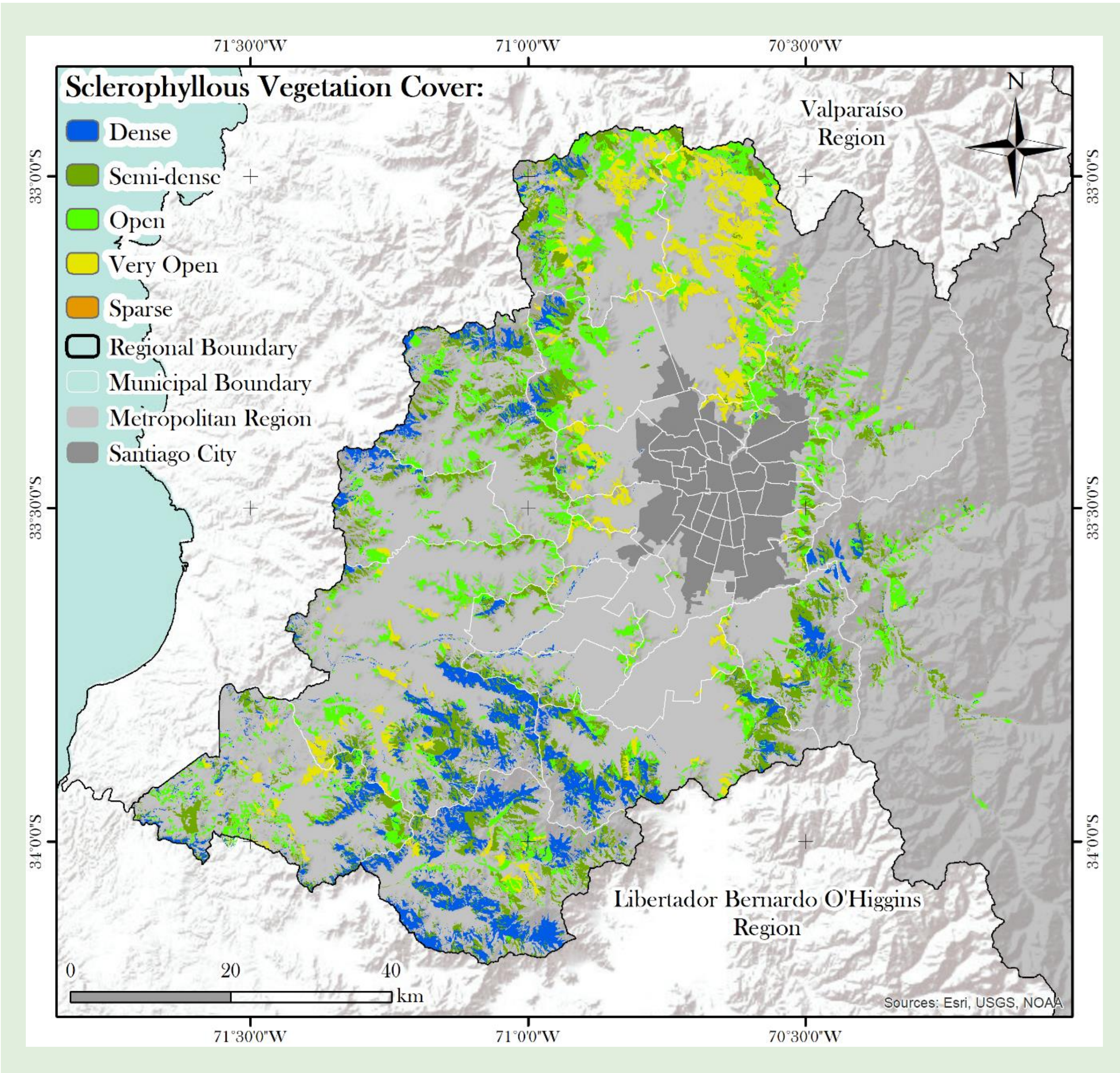

Figure 9. Spatial distribution of vegetation cover classes in the study-area sclerophyllous forest. Source: CONAF (2024).

has been documented mainly through NDVI, revealing long-term declines in canopy cover, productivity, and leaf area (Miranda et al., 2020, 2023; Fuentes et al., 2025). Indeed, previous studies analyzed temporal behavior of central Chilean sclerophyllous forest using MODIS-based NDVI products. Miranda et al. (2023) analyzed 250 m NDVI 16-day composites for 2000-2017, identifying negative trends in 10-38% of dense vegetation depending on forest subtype. Similarly, Fuentes et al. (2025) analyzed 500 m MODIS-derived products for 2001-2024 and detected rapid and widespread vegetation responses to the 2019-2020 extreme drought, with limited recovery affecting only ∼25% of the impacted area.

Although our study focused on a more geographically restricted area, its findings are consistent with those discussed above, showing widespread drought-related deterioration of sclerophyllous forests together with only partial vegetation recovery following prolonged dry conditions. Our study also provided several methodological contributions. It extended the retrospective period to 1985 and incorporated the ongoing precipitation recovery period, while enabling finer spatial analysis at 30 m resolution without prior forest-density filtering. Likewise, by classifying index-based standardized temporal slopes, it identified spatiotemporal deterioration patterns. Our results showed that the strongest deterioration tended to occur in denser vegetation cover at lower elevations and gentler slopes, particularly on southwestern aspects, where favorable moisture conditions foster denser vegetation, making these stands more vulnerable to drought. This pattern was particularly evident in Espino,

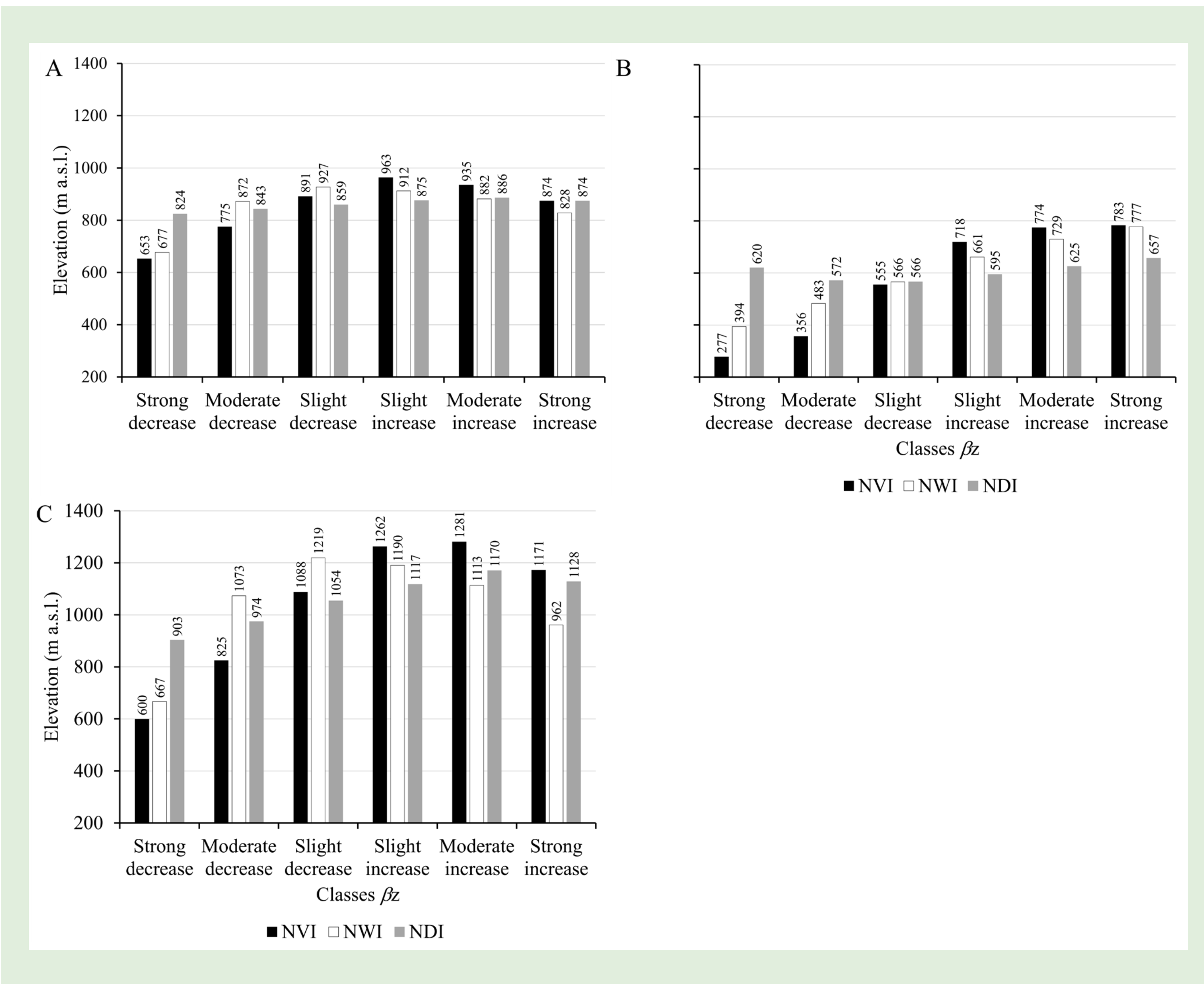

Figure 10. Mean elevation by temporal-change class of standardized spectral-index trends for Peumo-Quillay-Litre (PQL) (A), Espino (B), and Sclerophyllous (C).

which occupies lower elevations than the other subtypes, exhibiting stronger deterioration on flatter terrain. These findings suggest the combined influence of greater anthropogenic accessibility at lower elevations and greater vulnerability of denser stands under drought conditions. This is consistent with Schulz et al. (2011), who identified accessibility, mediated by slope and road proximity, as a key factor in historical sclerophyllous forest loss in central Chile, and with González-Reyes et al. (2024) and Fuentes et al. (2025), whose findings support the role of prolonged water deficits in driving deterioration of these Chilean forests.

These results underscore the importance of biotic-abiotic interactions in explaining sclerophyllous forest deterioration, particularly in the southwestern study area. Although the western Metropolitan Region experienced the greatest urban expansion in central Chile between 1975 and 2008, driven by industrial and infrastructure growth associated with Santiago and its conurbation north of the Maipo River valley (Schulz et al., 2010; Garreaud et al., 2025), the southwestern study area, encompassing the Coastal Range spurs, remained less affected by that expansion, retaining substantial forest remnants now exposed to progressive deterioration (CONAF, 2024).

The synergy between accumulated human pressure, as reflected by the confinement of forest fragments to increasingly restricted spaces, and chronic water stress intensified by the megadrought

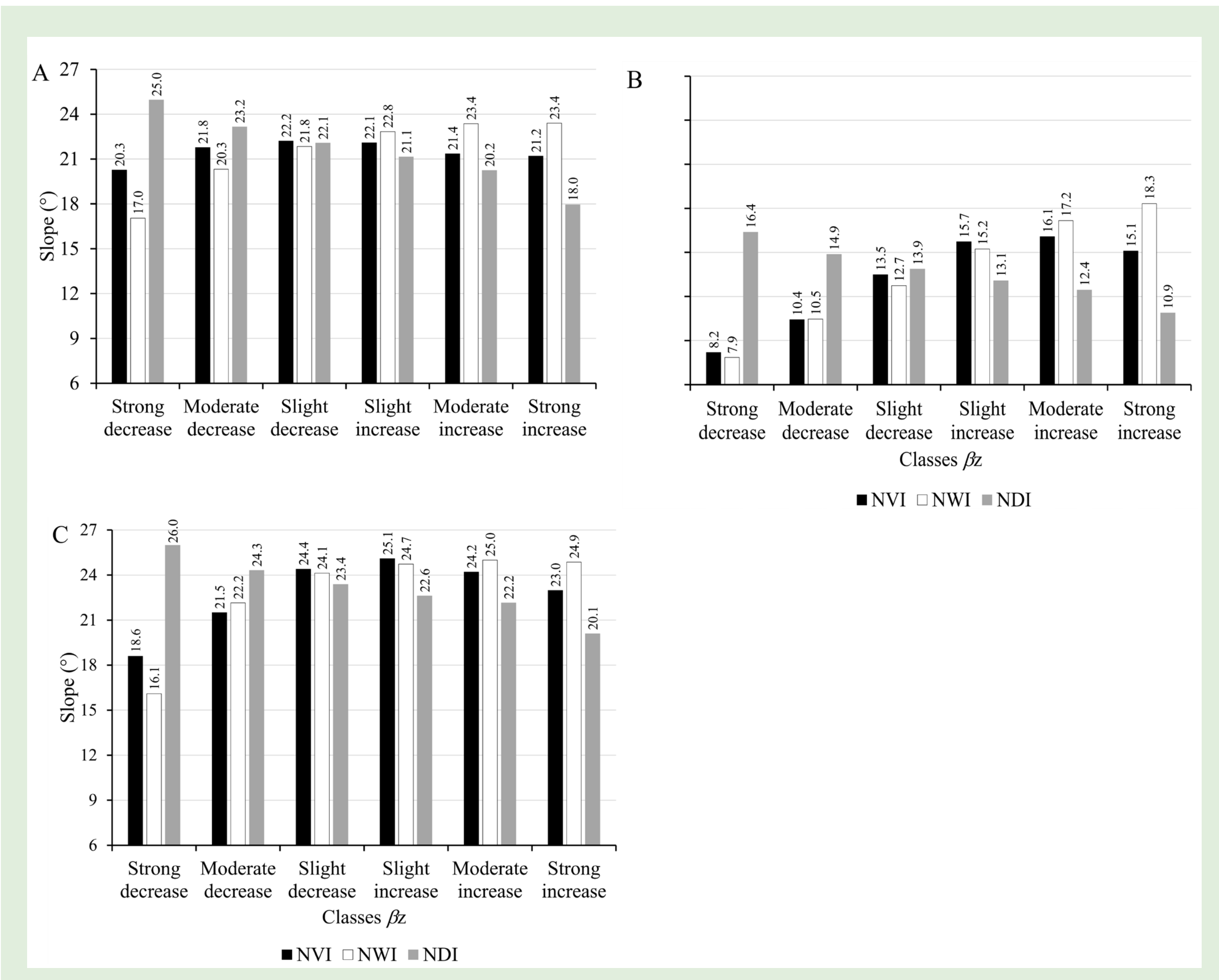

Figure 11. Mean slope by temporal-change class of standardized spectral-index trends for Peumo-Quillay-Litre (PQL) (A), Espino (B), and Sclerophyllous (C).

likely explains the spatiotemporal deterioration patterns identified in this study. Future research could strengthen these findings by extending the analysis to sclerophyllous forests deforested during the study period, particularly considering that the loss of these forests in central Chile has been estimated at 58% over the last decades (Schulz et al., 2010). Furthermore, short-term deterioration and recovery fluctuations that may be blurred by linear trends derived from a quinquennial-based sampling could be further explored using denser annual or seasonal image sets together with analytical approaches better suited to capturing short-term temporal dynamics. Lastly, the patterns identified here provide a foundation for process-based biophysical modeling aimed at establishing the biophysical interpretation of NDI. Consistent with the original development of NDDI, which called for broader evaluation of its index components across vegetation types and environmental settings (Gu et al., 2007), the NDI proposed here also requires dedicated biophysical validation, especially because it was formulated to adequately represent vegetation responses under the environmental setting of central Chile. Accordingly, such validation should integrate field observations with ecophysiological, meteorological, and hydrological measurements characterizing such a setting, complemented by remote sensing products describing canopy structure and vegetation condition (Mahmoud et al., 2025; Stamou et al., 2025). Such integration would help identify

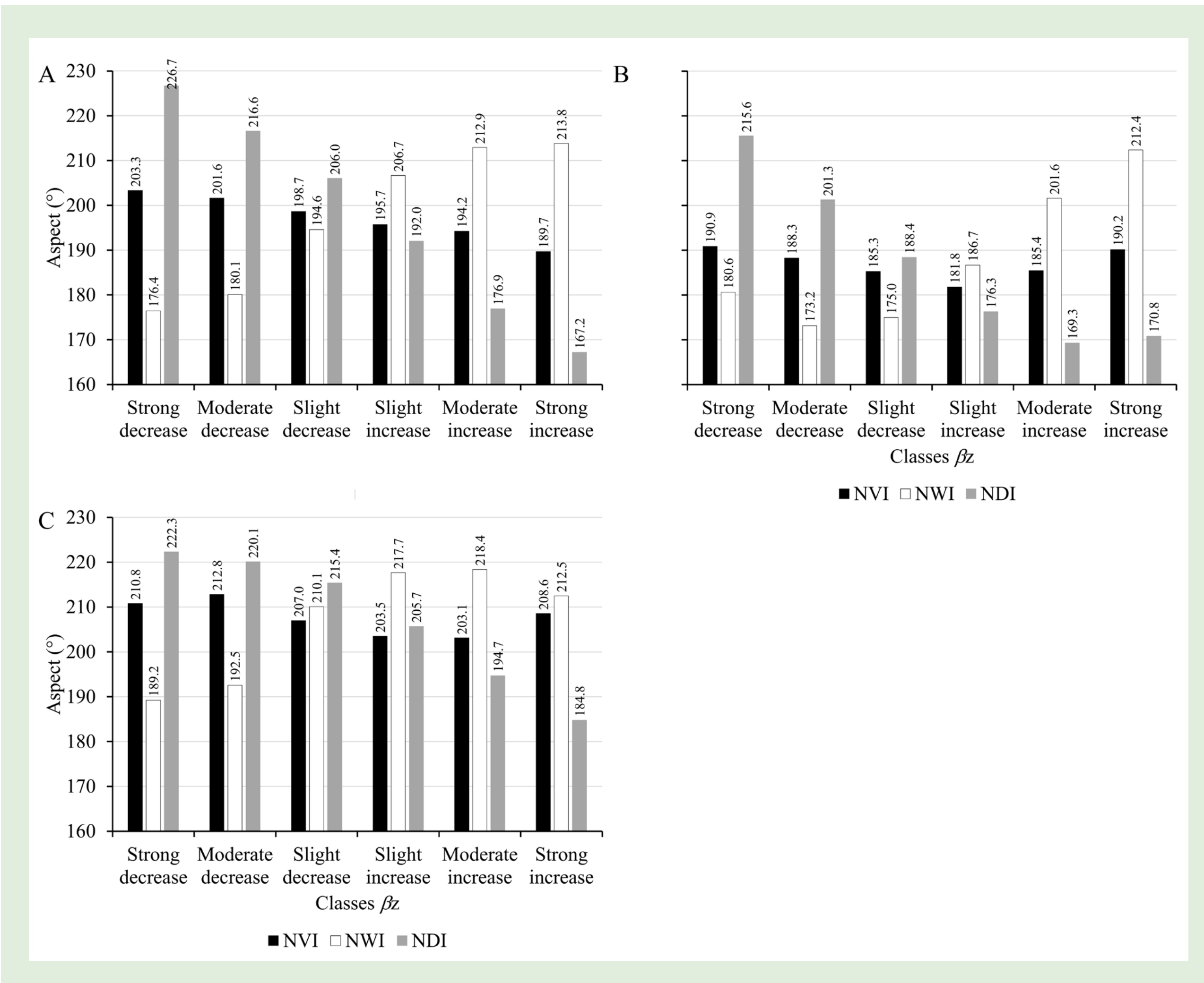

Figure 12. Mean aspect by temporal-change class of standardized spectral-index trends for Peumo-Quillay-Litre (PQL) (A), Espino (B), and Sclerophyllous (C).

Table 7. Statistical significance of differences between spectral-index temporal change classes and characterizing variables by forest subtype.

Variable	Spectral index	Forest subtype		
		Sclerophyllous	Espino	PQL
Terrain elevation	NVI	*** (49.06)	*** (82.76)	*** (171.3)
	NWI	*** (25.49)	*** (34.6)	*** (123.1)
	NDI	*** (5.60)	NS (2.15)	*** (11.67)
Terrain slope	NVI	** (15.80)	*** (55.1)	*** (193)
	NWI	*** (26.99)	*** (35.55)	*** (287.6)
	NDI	*** (16.00)	*** (6.14)	*** (79.82)
Terrain aspect	NVI	** (3.46)	NS (0.92)	* (2.36)
	NWI	*** (8.23)	NS (1.97)	*** (19)
	NDI	*** (17.52)	*** (3.53)	*** (34.7)
Vegetation cover	NVI	*** (160.38)	*** (156.86)	*** (1,271.2)
	NWI	*** (89.24)	*** (110.99)	*** (719.1)
	NDI	NS (24.37)	*** (81.7)	*** (302.54)

*** = P < 0.001. ** = P < 0.01. * = P < 0.05. NS = not significant (P > 0.05). F (ANOVA) and χ^2 (chi-square) values are shown in parentheses.

the biophysical processes governing NDI variability, strengthen its ecological interpretation, and define the environmental conditions under which it can be applied most reliably.

Conclusions

This study analyzed deterioration trends in the sclerophyllous forest of Chile's Metropolitan Region between 1985 and 2024 using modified NDVI, NDWI, and NDDI formulations. Classification of standardized temporal slopes by forest subtype enabled the identification of complementary spatiotemporal deterioration patterns associated with vegetation cover and topographic conditions at high spatial detail and broad temporal coverage. These patterns provide a useful framework for ecological and forest planning by helping to clarify where conservation and ecological restoration actions should be prioritized.

Applying a modified version of the NDDI to the eco-climatic context of central Chile enabled detection of variations in vegetation water stress affecting the sclerophyllous forest of the study area. Its sensitivity to marked deterioration during the 2020 megadrought peak, as well as its subsequent attenuation following precipitation recovery beginning in 2023, suggests potential for identifying climate-driven degradation processes in xeric ecosystems.

The most pronounced deterioration was concentrated in the southwestern study area, mainly affecting denser and more accessible stands at lower elevations and gentler slopes. This pattern occurred in areas historically subjected to intense anthropogenic pressure and is consistent with interactions between human disturbance and chronic water stress described for the study area.

Author contributions

The principal author (principal investigator and academic supervisor) conceptualized the study, designed the methodology, supervised data processing, and led manuscript preparation.

The co-author (research assistant and graduate student) led data processing and contributed to result interpretation and manuscript preparation.

Funding

This research received no specific funding.

AI use declaration

During the preparation of this manuscript, the authors made limited use of ChatGPT (GPT-5.6 Luna) to facilitate the explanation of methodologies described in some of the articles consulted in the study, review the grammar of the text body, and check the stylistic consistency of selected references. All AI-assisted content was reviewed and edited by the authors, who independently verified its accuracy and appropriateness and assume full responsibility for the final content of the publication.

REFERENCES

Centro de Información de Recursos Naturales. (2016). *DEM Alos Palsar Región Metropolitana*. Geoportal de Chile. https://geoportal.cl/geoportal/catalog/35439/DEM%20Alos%20Palsar%20Regi%C3%B3n%20Metropolitana

Corporación Nacional Forestal (CONAF). (2024). *Monitoreo de cambios, corrección gráfica y actualización del catastro de los recursos vegetacionales de la Región Metropolitana*. CONAF, Santiago, Chile. https://sit.conaf.cl

Dirección Meteorológica de Chile (DMC). (2026). *Servicios climáticos*. https://climatologia.meteochile.gob.cl/

Fuentes, I., Lopatin, J., Galleguillos, M., & McPhee, J. (2025). Vegetation browning as an indicator of drought impact and ecosystem resilience. *Science of Remote Sensing*, 11, 100219. https://doi.org/10.1016/j.srs.2025.100219

Gajardo, R. (1994). *La vegetación natural de Chile: clasificación y distribución geográfica*. Editorial Universitaria.

Gao, Y., Skutsch, M., Paneque-Gálvez, J., & Ghilardi, A. (2020). Remote sensing of forest degradation: A review. *Environmental Research Letters,* 15(10), 103001. https://doi.org/10.1088/1748-9326/abaad7

Garfias, R., Castillo, M., Ruiz, F., Vita, A., Bown, H., & Navarro, R. (2018). Remanentes del bosque esclerófilo en la zona mediterránea de Chile central: caracterización y distribución de fragmentos. *Interciencia,* 43(9), 655-663.

Garreaud, R. (2023). *Un breve recuento de las lluvias en la zona central de Chile ante la retirada de La Niña*. Centro de Ciencia del Clima y la Resiliencia (CR)2. https://www.cr2.cl/analisis-cr2-un-breve-recuento-de-las-lluvias-en-la-zona-central-de-chile-ante-la-retirada-de-la-nina/

Garreaud, R., Boisier, J. P., Alvarez-Garretón, C., Christie, D. A., Carrasco-Escaff, T., Vergara, I., Chávez, R. O., Aldunce, P., Camus, P., Suazo-Álvarez, M., Masiokas, M., Castro, G., Muñoz, A., Zambrano-Bigiarini, M., Fuster, R., & Godoy, L. (2025). Hyperdroughts in central Chile: drivers, impacts, and projections. *Hydrology and Earth System Sciences*, 29, 5347-5369. https://doi.org/10.5194/hess-29-5347-2025

González-Reyes, Á., Christie, D.A., Schneider-Valenzuela, I., Venegas-González, A., Muñoz, A.A., Hadad, M., Gipoulou-Zuñiga, T., Tapia-Marzan, V., Gibson-Carpintero, S., Santini-Junior, L., LeQuesne, C. & Villalba, R. (2024). Recent multispecies tree-growth decline reveals a severe aridity change in Mediterranean Chile. *Environmental Research Letters* 19, 064046. https://doi.org/10.1088/1748-9326/ad4049

Gu, Y., Brown, J. F., Verdin, J. P., & Wardlow, B. (2007). A five-year analysis of MODIS NDVI and NDWI for grassland drought assessment over the central Great Plains of the United States. *Geophysical Research Letters*, 34, L06407. https://doi.org/10.1029/2006GL029127

Hunt, E. R., Rock, B. N., & Nobel, P. S. (1987). Measurement of leaf relative water content by infrared reflectance. *Remote Sensing of Environment*, 22(3), 429-435. https://doi.org/10.1016/0034-4257(87)90094-0

Instituto Nacional de Estadísticas (INE). (2024). *Síntesis de resultados censo de población y vivienda 2024*. Instituto Nacional de Estadísticas.

Joseph, S., Murthy, M. S. R., & Thomas, A. P. (2011). The progress on remote sensing technology in identifying tropical forest degradation: a synthesis of the present knowledge and future perspectives. *Environmental Earth Sciences*, 64, 731-741. https://doi.org/10.1007/s12665-010-0893-8

Luebert, F., & Pliscoff, P. (2018). *Sinopsis bioclimática y vegetacional de Chile*. Editorial Universitaria.

Mahmoud, A. R., Farahat, E. A., Hassan, L. M., & Halmy, M. W. A. (2025). Remotely sensed data contribution in predicting the distribution of native Mediterranean species. *Scientific Reports*, 15, 12475. https://doi.org/10.1038/s41598-025-94569-y

Ministerio del Medio Ambiente (MMA). (2025). *Clasificación de especies*. MMA. https://clasificacionespecies.mma.gob.cl/

Miranda, A., Altamirano, A., Cayuela, L., Lara, A., & González, M. (2017). Native forest loss in the Chilean biodiversity hotspot: revealing the evidence. *Regional Environmental Change*, 17(1), 285-297. https://doi.org/10.1007/s10113-016-1010-7

Miranda, A., Altamirano, A., Cayuela, L., Pincheira, F., & Lara, A. (2015). Different times, same story: native forest loss and landscape homogenization in three physiographical areas of south-central Chile. *Applied Geography*, 60, 20-28. https://doi.org/10.1016/j.apgeog.2015.02.016

Miranda, A., Lara, A., Altamirano, A., Di Bella, C., González, M. E., & Camarero, J. J. (2020). Forest browning trends in response to drought in a highly threatened Mediterranean landscape of South America. *Ecological Indicators*, 115, 106401. https://doi.org/10.1016/j.ecolind.2020.106401

Miranda, A., Syphard, A. D., Berdugo, M., Carrasco, J., Gómez-González, S., Ovalle, J. F., Delpiano, C. A., Vargas, S., Squeo, F. A., Miranda, M. D., Dobbs, C., Mentler, R., Lara, A., & Garreaud, R. (2023). Widespread synchronous decline of Mediterranean-type forest driven by accelerated aridity. *Nature Plants*, 9, 1810-1817. https://doi.org/10.1038/s41477-023-01541-7

Peñuelas, J., Sardans, J., Filella, I., Estiarte, M., Llusià, J., Ogaya, R., Carnicer, J., Bartrons, M., Rivas-Ubach, A., Grau, O., Peguero, G., Margalef, O., Pla-Rabés, S., Stefanescu, C., Asensio, D., Preece, C., Liu, L., Verger, A., Barbeta, A., ... Terradas, J. (2017). Impacts of global change on Mediterranean forests and their services. *Forests, 8*(12), 463. https://doi.org/10.3390/f8120463

Rouse, J. W., Haas, R. H., Schell, J. A., & Deering, D. W. (1973). Monitoring vegetation systems in the Great Plains with ERTS. In *Third Earth Resources Technology Satellite Symposium*, 10-14 December 1973, 1(A), 309-317. Washington DC, USA. https://ntrs.nasa.gov/citations/19740022614

Salazar, A., Baldi, G., Hirota, M., Syktus, J., & McAlpine, C. (2015). Land use and land cover change impacts on the regional climate of non-Amazonian South America: A review. *Global and Planetary Change*, 128, 103-119. https://doi.org/10.1016/j.gloplacha.2015.02.009

Schulz, J. J., Cayuela, L., Echeverría, C., Salas, J., & Rey Benayas, J. M. (2010). Monitoring land cover change of the dryland forest landscape of Central Chile (1975-2008). *Applied Geography*, 30(3), 436-447. https://doi.org/10.1016/j.apgeog.2009.12.003

Schulz, J. J., Cayuela, L., Rey-Benayas, J. M., & Schröder, B. (2011). Factors influencing vegetation cover change in Mediterranean Central Chile (1975-2008). *Applied Vegetation Science*, 14, 571-582. https://doi.org/10.1111/j.1654-109X.2011.01135.x

Smith-Ramírez, C., Grez, A., Galleguillos, M., Cerda, C., Ocampo-Melgar, A., Miranda, M. D., Muñoz, A. A., Rendón-Funes, A., Díaz, I., Cifuentes, C., Alaniz, A., Seguel, O., Ovalle, J., Montenegro, G., Saldes-Cortés, A., Martínez-Harms, M. J., Armesto, J. J., & Vita, A. (2023). Ecosystem services of Chilean sclerophyllous forests and shrublands on the verge of collapse: A review. *Journal of Arid Environments,* 211, 104927. https://doi.org/10.1016/j.jaridenv.2022.104927

Stamou, A., Bakousi, A., Dosiou, A., Tsifodimou, Z.-E., Karachaliou, E., Tavantzis, I., & Stylianidis, E. (2025). Mapping drought incidents in the Mediterranean region with remote sensing: A step toward climate adaptation. *Land*, 14(8), 1564. https://doi.org/10.3390/land14081564

U.S. Geological Survey. (2026). *EarthExplorer*. https://earthexplorer.usgs.gov/

West, H., Quinn, N., & Horswell, M. (2019). Remote sensing for drought monitoring and impact assessment: Progress, past challenges and future opportunities. *Remote Sensing of Environment*, 232, 111291. https://doi.org/10.1016/j.rse.2019.111291